Ca^{2+} Activation of the $cPLA_2$ C2 Domain: Ordered Binding of Two Ca^{2+} Ions with Positive Cooperativity†

Nathan J. Malmberg,‡ Sameer Varma,# Eric Jakobsson,# and Joseph J. Falke*,‡

Molecular Biophysics Program, Department of Chemistry & Biochemistry, University of Colorado, Boulder, Colorado 80301-0215, and Center for Biophysics and Computational Biology, National Center for Supercomputing Applications, University of Illinois, Urbana, Illinois 61801

Received August 14, 2004; Revised Manuscript Received October 1, 2004

ABSTRACT: During Ca^{2+} activation, the Ca^{2+}-binding sites of C2 domains typically bind multiple Ca^{2+} ions in close proximity. These binding events exhibit positive cooperativity, despite the strong charge repulsion between the adjacent divalent cations. Using both experimental and computational approaches, the present study probes the detailed mechanisms of Ca^{2+} activation and positive cooperativity for the C2 domain of cytosolic phospholipase A_2, which binds two Ca^{2+} ions in sites I and II, separated by only 4.1 Å. First, each of the five coordinating side chains in the Ca^{2+}-binding cleft is individually mutated and the effect on Ca^{2+}-binding affinity and cooperativity is measured. The results identify Asp 43 as the major contributor to Ca^{2+} affinity, while the two coordinating side chains that provide bridging coordination to both Ca^{2+} ions, Asp 43 and Asp 40, are observed to make the largest contributions to positive cooperativity. Electrostatic calculations reveal that Asp 43 possesses the highest pseudo-pK_a of the coordinating acidic residues, as well as the highest general cation affinity, due to its relatively buried location within 3.5 Å of seven protein oxygens with full or partial negative charges. These calculations therefore explain the greater importance of Asp 43 in defining the Ca^{2+} affinity. Overall, the experimental and computational results support an activation model in which the first Ca^{2+} ion binds usually to site I, thereby preordering both bridging side chains Asp 40 and 43, and partially or fully deprotonating the three coordinating Asp residues. This initial binding event prepares the conformation and protonation state of the remaining site for Ca^{2+} binding, enabling the second Ca^{2+} ion to bind with higher affinity than the first as required for positive cooperativity.

The C2 domain is a ubiquitous membrane-targeting protein module found in a diverse array of signal transducing proteins that regulate key cellular processes at membrane surfaces (reviewed in refs *1*−*10*). These processes include the generation of lipid-derived second messengers, vesicular targetting and fusion, GTPase regulation, protein phosphorylation, pore formation by cytolytic T cells, and ubiquitin-mediated protein degradation. The majority of C2 domains are activated by cytoplasmic Ca^{2+} signals and dock to specific membrane-associated targets such as phospholipids or, less commonly, to membrane-bound proteins.

The structures of representative Ca^{2+}-regulated C2 domains, including the C2A domain of synaptotagmin I (Syt-IA),[1] the C2 domain of cytosolic phospholipase A_2 (α-isoform, $cPLA_2\alpha$), and the C2 domain of protein kinase C (PKC), have been determined by X-ray crystallography or NMR spectroscopy (*11*−*16*). These C2 domains are divided into two distinct topological classes termed Types I and II which share the same β-sandwich architecture but differ by a circular permutation in their pattern of β-strand connectivities (*7*). At one edge of the β-sandwich two or more Ca^{2+} ions bind with positive cooperativity in a cleft formed by three interstrand loops and lined with Ca^{2+}-coordinating side chains. These Ca^{2+}-binding loops are termed CBL I−III in order of their sequence in the primary structure. Together they provide Ca^{2+} coordination for up to four potential Ca^{2+}-binding sites labeled sites I−IV; however, in a given C2 domain only a subset of the four sites may actually bind Ca^{2+} in solution, since not all the sites provide adequate Ca^{2+} coordination. Thus, the Ca^{2+}-loaded C2 domains characterized to date possess from one to three Ca^{2+} bound in different combinations of sites I−IV (*12*, *15*, *17*−*19*).

The present study focuses on the C2 domain of $cPLA_2\alpha$, which upon Ca^{2+} activation docks to neutral lipids on the surface of specific intracellular membranes (*6*, *20*, *21*). Following docking, the separate catalytic domain hydrolytically releases arachidonic acid from lipid substrates, thereby triggering a variety of pathways including the inflammation response targeted by common anti-inflammatory drugs (*22*, *23*). The isolated $cPLA_2\alpha$ C2 domain is activated by the binding of two Ca^{2+} ions in solution with positive cooperativity, and this activation dramatically increases the affinity of the domain for membrane docking (*18*). High-resolution structures of the free domain reveal that the two bound Ca^{2+} ions occupy sites I and II of the four potential sites (*15*, *24*), but it is not known which of the two sites are

† Support provided by NIH Grants GM R01-063235 (to J.J.F.) and GM R01-054651 (to H.L.S./E.J.), and by a DOE/GTL Grant (to E.J.).

* Corresponding author: Tel 303-492-3503. Fax 303-492-5894. E-mail falke@colorado.edu.

‡ University of Colorado.

University of Illinois.

[1] Abbreviations: $cPLA_2\alpha$, the α-isoform of cytosolic phospholipase A_2; PKC, protein kinase C; Syt-I, synaptotagmin I; CBL, Ca^{2+}-binding loop; HEPES, *N*-(2-hydroxyethyl)piperazine-*N*′-2-ethanesulfonic acid.

10.1021/bi0482405 CCC: $27.50 © 2004 American Chemical Society
Published on Web 12/04/2004

loaded first during the activation process, and much remains to be learned about the mechanism of positive cooperativity for C2 domains in general. Such positive cooperativity is quite a remarkable feature of C2 domains, since these proteins typically bind multiple Ca^{2+} ions in close proximity where charge repulsion between the bound divalent cations is formidable. The existence of positive cooperativity indicates that despite this mutual repulsion the last Ca^{2+} ions bind more tightly than the first Ca^{2+} ion.

The only C2 domain for which a careful study of the order of Ca^{2+} binding has been undertaken is the C2A domain of synaptotagmin I, which binds three Ca^{2+} ions. NMR analysis of a Ca^{2+} titration revealed evidence that site I loads first with Ca^{2+}, followed by site II, and finally site III (*19*). (Note that it is coincidental that the order of binding follows the same sequence as the prior numbering of Ca^{2+}-binding sites in the structure). However, since different C2 domains utilize different combinations of sites I−IV to bind different numbers of Ca^{2+} ions, it is not yet clear whether the Ca^{2+}-binding order observed for the synaptotagmin C2A domain is relevant for other C2 domains. Moreover, no systematic study has yet tested the importance of specific coordinating side chains in the mechanism of positive cooperativity, although it has been suggested that bidentate aspartate side chains which simultaneously coordinate two Ca^{2+} ions could play a role in cooperativity between sites (*19*, *24*). To investigate the role of specific coordinating side chains in the Ca^{2+}-binding pocket of the $cPLA_2\alpha$ C2 domain, each of the five coordinating side chains has been substituted to eliminate its contribution to Ca^{2+} coordination. The effects of these substitutions on the affinity and cooperativity of Ca^{2+} binding have been quantitated using a fluorescence method to monitor the binding of two Ca^{2+} ions to the isolated C2 domain in solution. The results reveal the order of Ca^{2+} binding to the two sites, and indicate that Asp 43 is the most critical Ca^{2+} coordinating residue. In addition, computational analysis of pseudo-pK_a values for the three coordinating aspartate residues reveal that the negative charge of Asp 43 is highly destabilized by its local environment, which explains the central importance of this residue to Ca^{2+} affinity. Finally, the results indicate that the bridging residues Asp 40 and 43, which each coordinate both Ca^{2+} ions, are essential for positive cooperativity between the two Ca^{2+} sites. A molecular model based on both the experimental and computational findings is proposed to explain the importance of these bridging ligands to positive cooperativity.

METHODS

Protein Mutagenesis, Expression, and Purification. Single Cys mutants of the human $cPLA_2\alpha$ C2 domain (residues 1−138) were generated using the single-stranded mutagenesis technique of Kunkel et al. as previously described (*25*, *26*). Cys mutants were expressed as inclusion bodies in *Escherichia coli*, then were isolated, denatured, and refolded (*26*). Following refolding, each mutant was purified by FPLC size exclusion on a Superdex G-75 gel filtration column in purification buffer containing 100 mM KCl, 20 mM Tris pH 7.8 with HCl, and 1 mM $CaCl_2$. Analysis by polyacrylamide gel electrophoresis (PAGE) indicated that each mutant was at least 95% pure. Protein was snap-frozen in liquid N_2 and stored at −80 °C. Finally, immediately prior to Ca^{2+} affinity measurements, the protein was loaded onto a Chelex-100 resin column equilibrated with standard assay buffer containing 100 mM KCl, 20 mM *N*-(2-hydroxyethyl)-piperazine-*N*′-2-ethanesulfonic acid (HEPES), pH 7.4 with KOH. Passage over this column removed all bound and free Ca^{2+} from the protein sample, and replaced the purification buffer with standard assay buffer (*18*). The residual contaminating Ca^{2+} concentration is submicromolar (*18*).

Fluorescence Measurement of Ca^{2+} Binding. Equilibrium fluorescence experiments were carried out on a Photon Technology International QM-2000-6SE Fluorescence spectrometer at 25 °C. The intrinsic tryptophan fluorescence of Trp^{71} was monitored using excitation and emission wavelengths of $\lambda_{ex} = 284$ nm and $\lambda_{em} = 320$ nm, with excitation and emission slit width settings of 4 and 8 nm, respectively. A concentrated Ca^{2+} stock solution was titrated into the sample, generating an increase in the intrinsic Trp fluorescence as Ca^{2+} occupied its binding site (*18*). Samples contained 1.0 μM C2 domain in standard assay buffer as well as 5 mM dithiothreitol (DTT, ensuring that each mutant Cys residue was fully reduced).

The Ca^{2+} dependence of the fluorescence increase was quantified by plotting the fluorescence change (ΔF) as a function of free Ca^{2+} concentration ($[Ca^{2+}]$) and best-fitted using a Hill equation (*18*):

$$\Delta F = \Delta F_{max}\left(\frac{[Ca^{2+}]^H}{[Ca^{2+}]_{1/2}^{\ H} + [Ca^{2+}]}\right) \quad (1)$$

where ΔF_{max} represents the calculated maximal fluorescence change (normalized to 1.0 to facilitate comparison of different mutant samples), H represents the Hill coefficient, and $[Ca^{2+}]_{1/2}$ represents the free Ca^{2+} concentration that induces half-maximal fluorescence change. Best-fitting was carried out via nonlinear least-squares analysis in Kaleidagraph 3.5 (Synergy). Each titration was repeated at least once to ensure reproducibility.

pK_a Calculations: Overview. An energy minimization procedure was developed to optimize the locations of protons on Glu and Asp side chains that have two protonation sites and multiple torsion angles. This procedure optimizes proton positions based on an optimal sequence of protonation in which every successive proton is optimized in the context of the previously optimized protons. Subsequently, pK_a calculations were carried out in four steps. First, the energy minimization procedure was implemented and the proton positions of all Asp and Glu residues were optimized according to the most likely sequence of protonation. Second, for the three coordinating Asp side chains in the Ca^{2+}-binding pocket (Asp 40, 43, and 93), all possible protonation sequences were considered and the proton locations were optimized for each sequence, enabling calculation of a Boltzmann probability for each protonation sequence. Third, the pK_a of each coordinating Asp side chain was calculated by comparing the electrostatic energies of its protonated and unprotonated states, taking into account interactions with other titratable groups, partial charges, dielectric boundaries, and solvent. Fourth, the pK_a's determined for individual protonation sequences were averaged by weighting the contribution of each protonation sequence according to its calculated probability.

pK_a Calculations: Positioning Protons. The coordinates of the C2 domain of $cPLA_2\alpha$ were taken from the X-ray

crystallographic structure determined by Perisic, Williams and co-workers, PDB entry 1RLW (*14*). The missing hydrogen atoms (except the titratable protons on residues Glu and Asp) were added by globally optimizing the hydrogen-bond networks (*27*). Such an optimization has been shown to improve the results of a pK_a calculation (*28*).

The side chain carboxylate of Glu or Asp offers two protonation sites. The choice of protonation site and subsequent choice of the torsion angle COH can have a pronounced effect on the results of a pK_a calculation. Furthermore, these effects can be magnified if there are strong electrostatic interactions with other titratable residues. Thus, determining the optimum positions of the titratable protons is critical. To determine the optimum positions of these protons, we defined the energy of a titratable proton as follows:

$$E = E_{PE} + E_{torsional} \quad (2)$$

The first term E_{PE} is the electrostatic potential energy of the proton and the second term describes the effect of electron pairs of the carbonyl oxygen on the torsion angle of the O═C−O−H system about the C−O bond. In general, the latter term is negligible but is included for completeness. Describing the position of the proton in spherical coordinates relative to the position of a carboxylic oxygen atom, the above equation can be rewritten as:

$$E(r_{relative}(d,\theta,\phi)) = q_{proton}\phi(r_{relative}(d,\theta,\varphi))_{proton} + \left(-\frac{1.3}{2}\right)\cos(2\varphi) \quad (3)$$

where $d = 1$ Å is the distance between a titratable proton and its corresponding carboxylic oxygen; $\theta = 70.5°$ from an sp3 hybridization; φ is the torsion angle; ϕ_{proton} is the electrostatic potential at the position of the proton, and q_{proton} is the charge on the proton. In this equation, the cosine function used to describe the torsion energy term has been taken from the work of Alexov & Gunner (*29*). The electrostatic contribution to the total energy of the proton can be determined as a function of the torsion angle by solving the Poisson−Boltzmann equation for different positions of the proton. For each proton, the final selected location in space is that with the lowest relative energy.

A simple strategy of protonating each Asp and Glu residue independently (parallel protonation) can be applied only to cases where the addition of a proton to one residue does not affect the position of the proton on another residue. For cases where the protonation of one residue affects the position of the proton of another residue, different choices of protonation sequences can be expected to generate different protonated conformers. The Ca^{2+}-binding site of the cPLA$_2\alpha$ C2 domain has three proximal aspartates; thus multiple protonation sequences must be considered.

The proton energy E provides an estimate of the negative charge density on and around a specific oxygen atom. The higher the local negative charge density, the more likely the oxygen is to be protonated, and the lower the proton energy E. The protonation methodology must ensure that the oxygen protonated earlier in the process is the one for which the proton has the lowest relative energy. To achieve this objective, we developed a sequential protonation methodology. As a first step in this methodology, the torsion angle dependent energy functions of protons (given by eq 3) are determined for all Asp and Glu residues in the protein. This first set of energy function calculations are performed in the absence of all titratable protons on Asp and Glu residues. The residue protonated first is the one that has the lowest total energy in the entire first set of calculations, including contributions from partial charges, dielectric boundaries, and solvent effects as well as torsion angle energy contributions. A second set of torsion angle dependent energy function calculations is then performed in the presence of the added proton. The second proton is then added to the residue that has the lowest energy in the second set of calculations. This procedure is repeated until the last residue in the protein is protonated.

This method of protonating Asp and Glu residues ensures a reasonable ordering of protonation. For the titratable residues in the binding site, Asp 40, 43, and 93, a further refinement was implemented. For these residues, all possible permutations of ordering were considered. The probability of each permutation of protonation was calculated according to the following logic. For a particular assumed order of protonation, each proton is placed in its minimum energy state in the context of previous protonations, and the free energy of adding the proton is given by the grand partition function:

$$Z_1^r = \sum_{k=r+1}^{N} [\exp(\beta(\mu - E_{xk}^r))] \quad (4)$$

where N is the total number of titratable residues, μ is the chemical potential of the solution, β is the temperature factor $(kT)^{-1}$, and E_{xk}^r denotes the lowest energy of the titratable proton of residue xk when r residues have been protonated. The probability of the assumed order being correct is then given by the product of the probabilities of adding each successive proton. Using the partition function given by eq 4, the probability of correctness associated with a specific order ($x1 \rightarrow x2 \rightarrow ... \rightarrow xN$) can be easily derived as:

$$P(x1 \rightarrow x2 \rightarrow ... \rightarrow xN) = \prod_{j=1}^{N-1}\left(\frac{\exp(-\beta E_{xj}^{j-1})}{\sum_{k=j}^{N}\exp(-\beta E_{xk}^{j-1})}\right) \quad (5)$$

Since these probabilities map the magnitude of correctness onto the assumed orders of protonation and thereby onto different protonated conformers, they were subsequently used to weigh the pK_a's generated from using different protonated conformers.

The calculation of the electrostatic component of the proton energy for each given value of the torsion angle requires a discrete solution of the Poisson−Boltzmann equation. All these calculations were performed with the Poisson−Boltzmann equation solver of *UHBD* (*30*) using the following set of parameters: solvent dielectric constant of 80; protein dielectric constant of 2; PARSE charge-radii parameter sets (*31*); finest grid spacing of 0.1 Å probe radius of 1.4 Å (*32*); Stern layer of 2.0 Å; and an ionic strength of 100 mM.

pK_a Calculations: Electrostatic Environment of the Modeled Protons. pK_a calculations were performed utilizing an adaptation of the methodology embedded in the UHBD software package release 5.1 (*30*). The details of this methodology have been described elsewhere (*33*−*35*). In brief, the entire calculation was performed in two stages. In the first stage, we determined the free energy change associated with transferring each titratable residue from bulk solvent into its neutral protein environment. Such a free energy change includes changes in the electrostatic environment of the titratable residue arising from background protein partial charges and changes in dielectric boundaries and solvent accessibility. In the second stage, we determined interaction energies between all titratable residues. These interaction energies were then used along with the free energy changes calculated in the first stage to determine the most likely (Boltzmann weighted) partial charges of all titratable residue as a function of bulk pH. The pK_a of each residue was then defined as the pH at which it had a 50% chance of being protonated. This two-stage calculation was performed for all the protonated conformers generated using sequential protonation. The probabilities associated with each conformer (calculated from eq 5) were finally used to weight the conformer pK_a's when calculating the macroscopic pK_a, as reported in the text. These calculations were performed for a range of protein dielectric constants.

The calculation of pK_a of all residues in a protein requires multiple solutions of the Poisson−Boltzmann equation. The following parameters were used in solving the linearized form of the equation: solvent dielectric constant of 80; ionic strength of 100 mM; Stern layer of 2.0 Å; probe radius of 1.4 Å (*32*); one-half the OPLS Lennard-Jones σ values for atomic radii (*36*); united-atom charge parameter set from CHARMm version 22.0 (Molecular Simulations Inc. Waltham, MA, 1992); and a series of four focusing finite difference grids 57 × 57 × 57, 30 × 30 × 30, 36 × 36 × 36 and 50 × 50 × 50 with spacings of 2.0, 1.0, 0.5, and 0.25 Å, respectively, centered on the titrating site of interest.

All simulations for this paper were conducted on the IA-32 Linux cluster provided by the National Center for Supercomputing Applications (NCSA), Urbana-Champaign.

RESULTS

Mutagenesis of Coordinating Side Chains. Figure 1 illustrates the regulatory Ca^{2+}-binding cleft of the human $cPLA_2\alpha$ C2 domain (*24*). The two activating Ca^{2+} ions occupy adjacent binding sites I and II and are coordinated by five amino acid side chains, which each provide one (monodentate) or two (bidentate) coordinating oxygens: Asp 40 (bidentate, bridging Ca^{2+} I and II), Asp 43 (bidentate, bridging Ca^{2+} I and II), Asn 65 (monodentate, Ca^{2+} I), Asp 93 (bidentate, Ca^{2+} II), and Asn 95 (monodentate, Ca^{2+} II). To determine the relative importance of these side chains to the overall Ca^{2+}-binding affinity, each of the five residues was targeted for Cys substitution via site-directed mutagenesis. The Cys side chain is well-suited for the present study since it is smaller than the native coordinating Asp and Asn side chains and thus avoids steric clashes. Moreover, the Cys sulfhydryl does not coordinate Ca^{2+} due to its comparatively high pK_a and to the negligible affinity of sulfur ligands for Ca^{2+} (*37*).

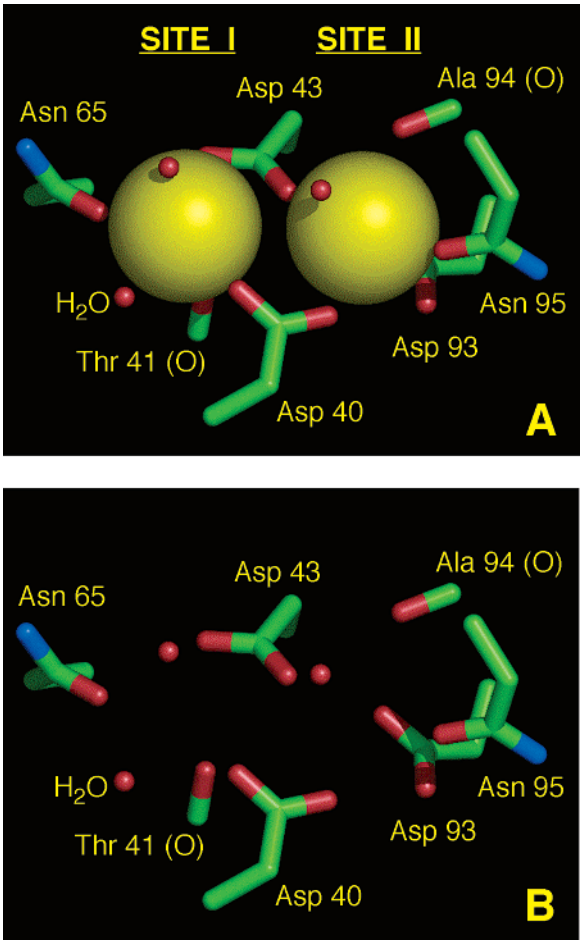

FIGURE 1: Ca^{2+}-binding cleft of the C2 domain of cytosolic phospholipase A2. (A) Shown is the crystallographically defined structure (*24*) of the Ca^{2+}-occupied cleft focusing on the two Ca^{2+} ions (large spheres) and the residues that provide Ca^{2+} coordination. The indicated coordinating oxygens (red) are provided both by protein residues (stick representations) and solvent oxygens (small spheres). Of the five coordinating side chains, two (Asp 40 and 43) donate bridging side chain carboxylates that each coordinate both Ca^{2+} ions. (B) Same structure with the two Ca^{2+} ions removed and the coordinating residues remaining fixed to provide a clear view of the coordinating residues. Figures generated using PyMol (DeLano Scientific).

The D40C, D43C, N65C, D93C, and N95C mutations were incorporated into the human $cPLA_2\alpha$ C2 domain gene by site-directed mutagenesis as previously described (*26*). The resulting mutant C2 domains were expressed in *E. coli* as inclusion bodies, then isolated, renatured, and purified by size exclusion chromatography to a level of 95% or greater for use in Ca^{2+}-binding studies. All five mutant proteins were fully water soluble and eluted at the same position on the Sephadex G75 size exclusion column as the wild-type protein, indicating that they were properly folded and monomeric.

Effects of Coordinating Side Chain Substitutions on Ca^{2+} Binding to the Free Domain. The $cPLA_2\alpha$ C2 domain possesses only one Trp residue, Trp 71, and the indole ring of this residue lies 12.6 and 12.0 Å from Ca^{2+}-binding sites I and II, respectively (*24*). Ca^{2+} binding to these sites is known to trigger a local structural change that increases the intrinsic emission of Trp 71 by 15%. The resulting fluorescence increase has been used previously to monitor the titration of sites I and II with two Ca^{2+} ions, yielding a

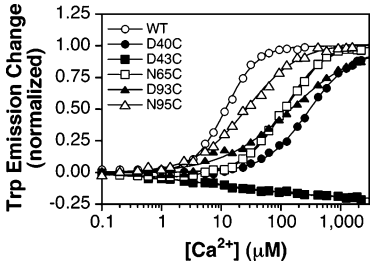

FIGURE 2: Ca^{2+}-binding profiles of mutant $cPLA_2\alpha$ C2 domains, each possessing a single Cys substitution at each of the five coordinating side chain positions. Profiles were determined at 25 °C by monitoring the intrinsic fluorescence change of Trp 71, and then were fitted with the Hill equation (eq 1, see Methods) to determine the best-fit apparent Ca^{2+} concentration that yields half-maximal binding ($[Ca^{2+}]_{1/2}$) and the best-fit Hill cooperativity coefficient (*H*). The resulting best-fit curves are indicated as solid lines, while the best-fit parameters are summarized in Table 2. Samples contained 1 μM free C2 domain, 100 mM KCl, 20 mM HEPES pH 7.4, and 5 mM DTT.

Table 1: Ca^{2+}-Binding Parameters of Coordinating Side Chain Mutants[a]

mutant	$[Ca^{2+}]_{1/2}$(Cys)/$[Ca^{2+}]_{1/2}$ (WT)	Hill coefficient (*H*)
WT	1	1.7 ± 0.2
D40C	21 ± 4	1.1 ± 0.1
D43C	$\gg 200$	n.d.
N65C	9 ± 2	1.4 ± 0.2
D93C	10 ± 3	0.8 ± 0.1
N95C	3 ± 1	1.8 ± 0.3

[a] Ca^{2+} concentrations required to give half-maximal binding ($[Ca^{2+}]_{1/2}$) and Hill cooperativity coefficients were determined at 25° C for each cysteine mutant (Cys) and wild type (WT) $cPLA_2\alpha$ C2 domain as described in Figure 2 and methods. The Ca^{2+} affinity change triggered by each mutation is indicated as the ratio of $[Ca^{2+}]_{1/2}$ values for the mutant and wild-type C2 domains. Samples contained 1 μM free C2 domain, 100 mM KCl, 20 mM HEPES pH 7.4, and 5 mM DTT. The dissociation constant of the wild-type C2 domain for Ca^{2+} is $K_D = 14 \pm 2$ μM.

$[Ca^{2+}]_{1/2}$ of 14 ± 2 μM and a Hill coefficient of 1.7 ± 0.2 (*6*, *18*). Since the Hill coefficient significantly exceeds 1.0, there is strong positive cooperativity between the two adjacent sites (*18*). The $[Ca^{2+}]_{1/2}$ and Hill coefficient measured using the fluorescence assay agree closely with the values determined by direct Ca^{2+} titration, validating the fluorescence method and confirming that the two binding sites contribute approximately equally to the fluorescence change (*6*, *18*).

The present study utilizes the intrinsic Trp fluorescence assay to monitor Ca^{2+} binding to the five coordination mutants, yielding the titration curves summarized in Figure 2. Best-fitting of the Hill equation to these titration curves in turn yields the $[Ca^{2+}]_{1/2}$ values and Hill coefficients summarized in Table 1. Following is an analysis of the effect of each coordination site substitution on the Ca^{2+}-binding properties of the C2 domain.

The D43C substitution yields the largest perturbation of Ca^{2+} binding. For this mutant, no detectable fluorescence increase is detected at Ca^{2+} concentrations as high as 1 mM, indicating that Ca^{2+} binding is no longer detectable and that modification of Asp 43 increases $[Ca^{2+}]_{1/2}$ at least 200-fold relative to the native C2 domain. Notably, Asp 43 is a bidentate ligand that simultaneously coordinates both Ca^{2+} ions in a bridging fashion (*24*). Moreover, of the five coordination mutants, Asp 43 mutant is the only one that fails to exhibit Ca^{2+}-triggered docking to phosphatidylcholine (PC) membranes in protein-to-membrane FRET studies (data not shown). Overall, since Asp 43 is the only coordinating position at which Cys substitution eliminates detectable Ca^{2+} binding and fully blocks Ca^{2+}-activated membrane docking, the results indicate that Asp 43 is the most important of the five coordinating side chains.

Smaller, but still significant, effects on Ca^{2+} binding are observed for the substitutions at the other two bidentate Asp positions, D40C and D93C. In the D40C mutant, modification of Asp 40 yields a 21-fold increase in $[Ca^{2+}]_{1/2}$ relative to the wild-type domain, indicating a large loss of Ca^{2+} affinity. In addition, the Hill coefficient decreases from 1.7 (for wild type) to 1.1, suggesting that most or all of the positive cooperativity between sites I and II is lost. Such a result is consistent with the possibility that either site I or II has been completely inactivated, such that the Ca^{2+}-binding stoichiometry has been reduced from 2 to 1 Ca^{2+} ions per domain. Like the Asp 43 residue, Asp 40 is a bidentate ligand that simultaneously coordinates both Ca^{2+} ions in a bridging fashion (*24*), thereby explaining its importance to Ca^{2+} binding in both sites I and II. However, the smaller effect of Asp 40 modification on Ca^{2+} binding indicates that it is not as critical as the Asp 43 residue, and that either site I or II retains the ability to bind a single Ca^{2+} ion.

In the D93C mutant, modification of Asp 93 yields a 10-fold increase in $[Ca^{2+}]_{1/2}$ relative to the wild-type domain, indicating a moderate loss of Ca^{2+} affinity. The Hill coefficient also decreases from 1.7 (for wild type) to 0.8, suggesting the complete loss of the positive cooperativity between sites I and II. These findings are consistent with the possibility that either site I or II has been fully inactivated, thereby reducing the Ca^{2+}-binding stoichiometry of the domain from two to one Ca^{2+} ions per domain. Like the two other Asp residues discussed above, Asp 93 is bidentate, but unlike the previous examples Asp 93 is not a bridging ligand. Instead, both Asp 93 carboxylate oxygens coordinate the Ca^{2+} ion bound in site II (*24*). Thus, it is site II that is most likely inactivated by the loss of Asp 93, thereby accounting for the absence of positive cooperativity.

Significant effects on Ca^{2+} binding are also observed for the N65C and N95C substitutions. In the N65C mutant, modification of Asn 65 increases $[Ca^{2+}]_{1/2}$ by a factor of 9-fold relative to the wild-type domain, indicating a moderate loss of affinity. The Hill coefficient of 1.4 indicates that modification of Asn 65 retains the positive cooperativity between sites I and II, and thus that the domain retains the binding of two Ca^{2+} ions. Unlike the coordinating Asp side chains, Asn 65 is monodentate and provides only one coordinating oxygen to the Ca^{2+} ion bound in site I (*24*), thereby explaining the smaller effects observed for this substitution.

In the final mutant N95C, modification of Asn 95 increases $[Ca^{2+}]_{1/2}$ by a factor of only 3-fold relative to wild type and retains the native Hill coefficient of 1.8. It follows that modification of this position yields the smallest effects on Ca^{2+} binding observed for the five coordinating side chains. Like Asn 65, the Asn 95 side chain provides monodentate coordination, but Asn 95 is a ligand to the Ca^{2+} in site II (*24*).

Together, the effects of amino acid replacement at the five coordinating side chain positions provide strong evidence

that site I plays a more important role than site II in defining the structure and $[Ca^{2+}]_{1/2}$ of the cooperative binding site pair. This conclusion is supported by the observation that replacement of the monodentate Asn 95 ligand in site II has the smallest effect on Ca^{2+} binding, while the corresponding replacement of monodentate Asn 65 in site I causes a 3-fold larger increase in the $[Ca^{2+}]_{1/2}$. Moreover, the replacement of monodentate Asn 65 in site I causes nearly the same Ca^{2+} affinity loss as the replacement of bidentate Asp 93 in site II, despite the fact that the latter residue provides two coordinating oxygens. In summary, site I is more critical than site II in the binding site pair, while the bidentate, bridging Asp 43 carboxylate that coordinates the adjacent Ca^{2+} ions in both sites is the most important of the five side chain ligands and is essential for Ca^{2+} binding to both sites. The experimental results do not, however, explain why Asp 43 is more important than Asp 40, which also serves as a bidentate ligand that bridges the two Ca^{2+} ions. To investigate this question, pK_a calculations were carried out for the three coordinating Asp side chains to investigate their electrostatic environments.

Calculation of Pseudo-pK_a's for the Coordinating Aspartates. The microscopic affinity of a given Asp carboxylate for Ca^{2+} will depend in part on the local electrostatic environment, which modulate the stability of the Asp negative charge. When the negative charge is destabilized by local electrostatic fields, the Asp will typically exhibit a higher affinity for Ca^{2+}. Such a destabilized carboxylate will also exhibit higher affinity for protons; thus, knowledge of the proton affinity of the coordinating carboxylates can identify which carboxylates make the largest contributions to Ca^{2+} affinity. Here we focus solely on the relative cation affinities of the three coordinating carboxylates in the Ca^{2+}-occupied state of the binding pocket. Since the relevant electrostatic environment of each coordinating carboxylate is that experienced in the Ca^{2+}-occupied structure of the pocket, the Gedanken approach began by removing the Ca^{2+} ions from the crystal structure of the Ca^{2+}-occupied C2 domain while fixing the coordinating residues in their Ca^{2+}-binding conformations (Figure 1B). Subsequently, this pseudo-structure was used to calculate a pseudo-pK_a for each coordinating carboxylate. The pseudo-pK_a is different from the true pK_a of each carboxylate in the apo protein, since the true pK_a is defined by the fee energy change associated with protonating that carboxylate in the true structure of the apo site, which is unknown but is undoubtedly different than the pseudo-structure utilized herein. However, the pseudo-structure and its corresponding pseudo-pK_a's are useful in comparing the relative affinities of the coordinating carboxylates in the Ca^{2+}-occupied binding pocket. Subsequently, hydrogens were added to all nontitratable moieties and protons were added to all titratable groups, including the side chain carboxylates of coordinating Asp residues 40, 43, and 93. To determine the optimal locations of the protons on titratable groups, a most-likely hydrogen-bond network was obtained by positioning protons of all Asp and Glu residues within the C2 domain using a proton-energy guided sequential protonation procedure (see Methods). For the aspartates in the Ca^{2+}-binding pocket of the C2 domain of cPLA$_2\alpha$, this protocol resulted in the following relative order of protonation: first protonation of Asp43, followed by protonation of Asp40, followed by protonation of Asp93 (Asp43 → Asp40 → Asp93). The protonated model that was a result of this sequence of protonation is shown as conformer 1 in Figure 3.

Protonation Sequences	
1	43 40 93
2	43 93 40
3	40 43 93
4	40 93 43
5	93 40 43
6	93 43 40
7	parallel

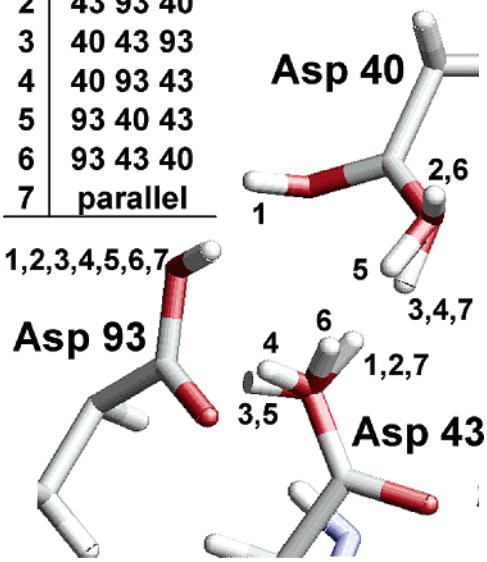

FIGURE 3: Modeled protonation states of the three coordinating aspartate side chains. Shown are the side chains of coordinating Asp residues 40, 43, and 93, including the optimized proton positions utilized by six separate pseudo-pK_a calculations in which protons are added consecutively to each of the three carboxylates. The side chains are constrained in a pseudo-structure generated by removing the two Ca^{2+} ions from the crystal structure conformation of the binding pocket, while fixing the side chains in their Ca^{2+}-binding positions. The inset table indicates the order of proton addition for each of the six protonation models, while the small numbers on each side chain indicate the proton positions used for these models.

But these three residues can also be protonated in five other possible relative orders. To generate protonated models using the five other sequences of protonation, we made the following assumption. We assumed that the titratable protons of aspartates or glutamates outside the binding site would not affect the positions of protons on these three residues. The titratable protons of Asp40, Asp43, and Asp93 were then removed from conformer 1 and the five sequences of protonation of the three aspartates were enforced (preset) to generate five separate conformers. These conformers labeled as 2, 3, 4, 5, and 6 are shown overlaid on conformer 1 in Figure 3.

The probability that these three residues would be protonated in a given order was calculated using a reduced form of eq 5. For three residues *i*, *j* and *k*, and for the probability that residue *i* is protonated before *j* and residue *j* before *k*, eq 5 reduces to a product of two terms

$$\boldsymbol{P}(i \rightarrow j \rightarrow k) = \frac{\exp(-\beta E_i^0)}{\exp(-\beta E_i^0) + \exp(-\beta E_j^0) + \exp(-\beta E_k^0)} \times \frac{\exp(-\beta E_j^1)}{\exp(-\beta E_j^1) + \exp(-\beta E_k^1)} \quad (6)$$

Table 2: Probabilities of the Six Possible Sequences of Protonation[a]

sequence of protonation	probability $P(i \rightarrow j \rightarrow k)$	resulting conformer no.
Asp43 → Asp40 → Asp93	0.46	1
Asp43 → Asp93 →Asp40	0.40	2
Asp40 → Asp43 → Asp93	0.06	3
Asp40 → Asp93 → Asp43	0.04	4
Asp93 → Asp40 → Asp43	0.02	5
Asp93 → Asp43 → Asp40	0.02	6

[a] For the three coordinating aspartates in sites I and II, the probability of each indicated protonation sequence was calculated using eq 6 (see methods). Since a given protonation sequence generates a unique set of conformational optimizations in a path-dependent fashion, each protonation sequence yields a different final conformation and hydrogen-bond network for the coordinating aspartates.

Table 3: Averaged Pseudo-pK_a Values for the Aspartates in the C2 Domain Ca^{2+}-Binding Pocket[a]

	weighted average of pseudo-pK_a		
residue	PD constant = 8	PD constant = 12	PD constant = 16
Asp 40	6.3	5.4	5.1
Asp 43	12.0	9.2	8.4
Asp 93	10.6	10.2	8.8

[a] Calculations were carried out for indicated values of the protein dielectric (PD) constant, based on a pseudo-structure of the Ca^{2+}-binding pocket in which the two Ca^{2+} ions were removed from the crystal structure of the Ca^{2+}-occupied C2 domain (*24*), and titratable protons were then added using the six different sequences of protonation (Table 2). The pseudo-pK_a values resulting from each of the six conformers were averaged using weights listed in Table 2.

The probabilities that these three aspartates would be protonated in each of the six possible consecutive orders are listed in Table 2.

Pseudo-pK_a's were then separately calculated for each of the six protonated models assuming values for the protein dielectric constants (8, 12, and 16) that are significantly larger than those typically used for an electrostatic description of protein interiors. These moderate values of protein dielectric constant implicitly account for penetration of water into the Ca^{2+}-binding pocket (*38*) and also help account for the conformational relaxation of flexible side chains (*39*, *40*). It is important to note that these are not the dielectric constants of the protein, but are used to implicitly absorb the effects of certain phenomena that are not explicitly modeled in the calculation of pK_a. The pseudo-pK_a values resulting from each of the six conformers were then averaged using the probabilities listed in Table 2 as weights. The weighted averages of pseudo-pK_a for different assumptions of the protein dielectric constant are listed in Table 3.

The calculated pseudo-pK_a values reveal the importance of electrostatic factors in the Ca^{2+}-binding roles of Asp 43, Asp 40, and Asp 93. Notably, Asp 43 consistently exhibits a higher pseudo-pK_a than either Asp 40 or Asp 93, indicating that the negative charge of its carboxylate is more destabilized by the local environment. Examination of the structure (*24*) reveals the sources of this destabilization: the Asp 43 carboxylate is more sequestered from solvent than those of Asp 40 and 93, and is within 3.5 Å of seven carboxylate and carbonyl oxygens (D40 OD1, D40 OD2, T41 O, P42 O, N65 OD1, D93 OD1, A94 O). The high pseudo-pK_a of Asp 43 further indicates that it would have the highest general cation affinity of the coordinating side chains. Such a high cation affinity, plus its bridging position between sites I and II, fully explain the observation that Asp 43 is the most important Ca^{2+}-coordinating ligand. By contrast, Asp 40, the only other bridging ligand, consistently exhibits the lowest pseudo-pK_a in the calculations and thus possesses a significantly lower cation affinity than Asp 43. Thus, the different electrostatic environments of Asp 43 and Asp 40 explain the smaller contribution of the latter to Ca^{2+} affinity. The remaining ligand, Asp 93, is bidentate like Asp 43 and Asp 40, and it possesses a consistently higher pseudo-pK_a than Asp 40 indicating a higher cation affinity. However, the observation that Asp 40 plays a greater role in defining Ca^{2+} affinity than Asp 93 indicates that the bridging position of Asp 40, as well as its contributions to site I, outweigh the contributions of Asp 93 to site II in the overall binding of two Ca^{2+} ions.

In the Ca^{2+}-occupied site, the three coordinating Asp residues are fully deprotonated to provide bidentate coordination in sites I and II; however, the pseudo-pK_a's calculated in the absence of Ca^{2+} emphasize that the apo binding pocket would be partially protonated if the residues within the pocket remain fixed in their Ca^{2+}-coordinating positions. In this case, the calculations performed for dielectric constants of 8 and 12, which are reasonable values for a ligand binding cleft within a protein, indicate that the three Asp residues would bind from 1 to 2 protons in the absence of bound cations. More likely, the coordinating side chains would relax to conformations different from their Ca^{2+}-coordinating state to optimize their electrostatic environment of the apo binding pocket, so that the calculated number of bound protons is an upper limit. As a result, the net negative charge of the apo pocket is between -3 and -1 eu. By contrast, when the pocket is loaded with two Ca^{2+} ions, the three coordinating Asp residues are fully deprotonated to provide bidentate coordination, but the positive charge of the two divalent cations ($+4$ eu) completely cancels the coordinating negative charge (-3 eu), yielding a net positive charge of $+1$ eu. These findings indicate that in a cellular setting, the Ca^{2+}-binding pocket switches from a negatively charged "off" state to a positively charged "on" state when it is loaded with two divalent cations during a Ca^{2+} signal. Such findings have important implications for a molecular understanding of the electrostatic switch that controls, at least in part, membrane docking.

DISCUSSION

The experimentally determined effects of coordinating side chain substitutions on Ca^{2+} binding to the cPLA$_2\alpha$ C2 domain reveal the relative importance of the site I and site II coordinating residues in the binding of two Ca^{2+} ions. Site I plays a more important role in defining the macroscopic Ca^{2+} affinity, since the $[Ca^{2+}]_{1/2}$ is 3-fold more sensitive, on a per-oxygen basis, to replacement of coordinating oxygens in site I than in site II. Thus, substitution of monodentate Asn 65 in site I causes a 3-fold greater Ca^{2+} affinity loss than the equivalent substitution of monodentate Asn 95 in site II. Similarly, substitution of Asn 65 in site I causes a 3-fold greater affinity loss than the substitution of either of the two Asp 93 coordinating oxygens in site II, assuming that the Ca^{2+} affinity loss due to replacement of bidentate Asp 93 stems from equal contributions of its two coordinating oxygens. The simplest model consistent with

these findings is an ordered binding model in which the first Ca^{2+} ion typically binds to site I and the second Ca^{2+} ion binds to site II, since for a cooperative binding site pair the site that loads first with ligand largely defines the apparent ligand affinity. However, because the loss of coordinating oxygens in site I and II exhibit only a modest 3-fold difference in their effects on Ca^{2+} affinity, it is likely that the ordered binding mechanism is not perfect, such that the first Ca^{2+} ion will sometimes bind first to site II rather than site I.

The findings provide the first experimental support for the hypothesis that the bridging ligands Asp 40 and 43 play an essential role in positive cooperativity (*24*). Loss of Asp 40 is observed to eliminate positive cooperativity, while loss of Asp 43 eliminates all detectable Ca^{2+} binding. A simple mechanism that explains the role of these two side chains in cooperativity begins with the apo site, wherein charge repulsion between the coordinating Asp carboxylates ensures that they are partially protonated and generally not in their Ca^{2+}-binding orientations (*37*). The binding of the first Ca^{2+} ion, either to site I or II, drives the conformations of the bridging side chains Asp 40 and 43 into their Ca^{2+}-binding positions. At the same time, the binding of the first Ca^{2+} ion partially or completely deprotonates the three Asp residues. Together these events triggered by the binding of the first Ca^{2+} ion prepare the structure and protonation state of the remaining site for the second Ca^{2+}-binding event. As a result of this preordering, the second Ca^{2+} ion is able to bind with higher affinity than the first, accounting for the strong positive cooperativity between the two sites. The magnitude of this positive cooperativity is especially striking given the close proximity of the two Ca^{2+} ions, which generates considerable electrostatic repulsion between the two divalent cations. Since Ca^{2+} usually binds first to site I, it is primarily site I that defines the overall Ca^{2+} affinity, while site II usually binds the second Ca^{2+} ion and benefits from the preorganization provided by prior Ca^{2+} binding to site I.

The most important coordinating ligand is Asp 43, which is the only coordinating side chain essential for Ca^{2+} binding to both sites I and II. The strong contribution of Asp 43 to the Ca^{2+} affinity arises partly from its structural role as a bridging ligand, since it provides coordination to Ca^{2+} ions in both sites I and II and contributes to the positive cooperativity between the two sites. In addition, pseudo-pK_a calculations carried out for the apo binding pocket with the coordinating residues fixed in their Ca^{2+}-binding positions, indicate that the local electrostatic environment destabilizes the negative charge of the Asp 43 carboxylate, thereby substantially increasing its general cation affinity relative to the other coordinating Asp residues. This destabilization results from a more buried location as well as proximity of the Asp 43 carboxylate to seven carboxylate and carbonyl oxygens within 3.5 Å. As a result of its central importance, Asp 43 is the only one of the five coordinating side chains for which substitution completely eliminates Ca^{2+} binding to both sites I and II, as well as Ca^{2+}-activated membrane docking.

Finally, the pseudo-pK_a calculations for three coordinating Asp side chains in sites I and II indicate that in the absence of bound cations, with the coordinating residues fixed in their Ca^{2+}-binding positions, at least two of the Asp side chains are partially or fully protonated. It is worth noting that this result was also provided by calculations carried out for the protonation model generated by a simultaneous protonation of all aspartates (shown as conformer 7 in Figure 3). These calculations suggest that the apo binding pocket could retain up to 1 to 2 bound protons, yielding a net charge for the pocket of -3 to -1 eu. As a result, the negative charge of the three coordinating Asp residues is not fully developed until two Ca^{2+} ions bind, at which point the three Asp carboxylates are fully deprotonated so that they can serve as bidentate ligands. When the binding pocket is filled with two divalent cations such as Ca^{2+}, the net charge becomes positive at $+1$ eu. Thus, in a resting cell prior to a Ca^{2+} signal, the apo binding pocket possesses a net negative charge, and switches to a net positive charge upon Ca^{2+} loading. Notably, the pseudo-pK_a calculations indicate that electrostatic switch models must take into account the significant protonation state of the apo C2 domain before Ca^{2+} binds, which reduces the magnitude of the Ca^{2+}-triggered electrostatic change available for regulation of membrane docking. The reduced magnitude of this electrostatic switch increases the relative importance of other activation mechanisms, particularly the direct or indirect coordination of the two Ca^{2+} in the binding pocket by lipid headgroup oxygens upon membrane docking. Evidence supporting the essential roles of both the electrostatic switch activation mechanism and the coordinating lipid activation mechanism is now available for C2 domains, suggesting that both mechanisms contribute to Ca^{2+}-activated membrane docking (*5*, *6*, *14*, *41*−*45*).

To fully understand Ca^{2+}-activated membrane docking, high-resolution structural information is needed for the Ca^{2+}-loaded C2 domain docked to the membrane surface. Considerable information is now available regarding the structure of the protein−membrane complex formed when the $cPLA_2\alpha$ C2 domain binds to a lipid bilayer: EPR studies have revealed the depth of C2 domain penetration into the membrane and the angle of the domain relative to the membrane surface (*1*, *46*). However, nothing is yet known about the effects of protein insertion on local lipid structure, which must be significantly perturbed. To define the effects of protein insertion on the positions and conformations of the surrounding lipid molecules, it will again be necessary to employ both experimental and computational methods to develop a more complete molecular picture of the protein-membrane interface.

REFERENCES

1. Malmberg, N. J., Van Buskirk, D. R., and Falke, J. J. (2003) Membrane docking loops of the cPLA2 C2 domain: Detailed structural analysis of the protein-membrane interface via site-directed spin labeling, *Biochemistry 42*, 13227−13240.
2. Hurley, J. H. (2003) Membrane proteins. Adapting to life at the interface, *Chem. Biol. 10*, 2−3.
3. Hurley, J. H., and Meyer, T. (2001) Subcellular targeting by membrane lipids, *Curr. Opin. Cell Biol. 13*, 146−152.
4. Tomsig, J. L., and Creutz, C. E. (2002) Copines: a ubiquitous family of Ca(2+)-dependent phospholipid-binding proteins, *Cell Mol. Life Sci. 59*, 1467−1477.
5. Kohout, S. C., Corbalan-Garcia, S., Torrecillas, A., Gomez-Fernandez, J. C., and Falke, J. J. (2002) C2 domains of protein kinase C isoforms alpha, beta, and gamma: activation parameters and calcium stoichiometries of the membrane-bound state, *Biochemistry 41*, 11411−11424.

6. Nalefski, E. A., Wisner, M. A., Chen, J. Z., Sprang, S. R., Fukuda, M., Mikoshiba, K., and Falke, J. J. (2001) C2 domains from different Ca^{2+} signaling pathways display functional and mechanistic diversity, *Biochemistry 40*, 3089−3100.
7. Nalefski, E. A., and Falke, J. J. (1996) The C2 domain calcium-binding motif: structural and functional diversity, *Protein Sci. 5*, 2375−2390.
8. Cho, W. (2001) Membrane targeting by C1 and C2 domains, *J. Biol. Chem. 276*, 32407−32410.
9. Rotin, D., Staub, O., and Haguenauer-Tsapis, R. (2000) Ubiquitination and endocytosis of plasma membrane proteins: role of Nedd4/Rsp5p family of ubiquitin-protein ligases, *J. Membr. Biol. 176*, 1−17.
10. Edwards, A. S., and Newton, A. C. (1997) Regulation of protein kinase C betaII by its C2 domain, *Biochemistry 36*, 15615−15623.
11. Sutton, R. B., Davletov, B. A., Berghuis, A. M., Sudhof, T. C., and Sprang, S. R. (1995) Structure of the first C2 domain of synaptotagmin I: a novel Ca^{2+}/phospholipid-binding fold, *Cell 80*, 929−938.
12. Sutton, R. B., and Sprang, S. R. (1998) Structure of the protein kinase Cbeta phospholipid-binding C2 domain complexed with Ca^{2+}, *Structure 6*, 1395−1405.
13. Shao, X., Fernandez, I., Sudhof, T. C., and Rizo, J. (1998) Solution structures of the Ca^{2+}-free and Ca^{2+}-bound C2A domain of synaptotagmin I: does Ca^{2+} induce a conformational change? *Biochemistry 37*, 16106−16115.
14. Davletov, B., Perisic, O., and Williams, R. L. (1998) Calcium-dependent membrane penetration is a hallmark of the C2 domain of cytosolic phospholipase A2 whereas the C2A domain of synaptotagmin binds membranes electrostatically, *J. Biol. Chem. 273*, 19093−19096.
15. Xu, G. Y., McDonagh, T., Yu, H. A., Nalefski, E. A., Clark, J. D., and Cumming, D. A. (1998) Solution structure and membrane interactions of the C2 domain of cytosolic phospholipase A2, *J. Mol. Biol. 280*, 485−500.
16. Dessen, A., Tang, J., Schmidt, H., Stahl, M., Clark, J. D., Seehra, J., and Somers, W. S. (1999) Crystal structure of human cytosolic phospholipase A2 reveals a novel topology and catalytic mechanism, *Cell 97*, 349−360.
17. Essen, L. O., Perisic, O., Lynch, D. E., Katan, M., and Williams, R. L. (1997) A ternary metal binding site in the C2 domain of phosphoinositide-specific phospholipase C-delta1, *Biochemistry 36*, 2753−2762.
18. Nalefski, E. A., Slazas, M. M., and Falke, J. J. (1997) Ca^{2+}-signaling cycle of a membrane-docking C2 domain, *Biochemistry 36*, 12011−12008.
19. Ubach, J., Zhang, X., Shao, X., Sudhof, T. C., and Rizo, J. (1998) Ca^{2+} binding to synaptotagmin: how many Ca^{2+} ions bind to the tip of a C2-domain? *Embo J. 17*, 3921−3930.
20. Nalefski, E. A., McDonagh, T., Somers, W., Seehra, J., Falke, J. J., and Clark, J. D. (1998) Independent folding and ligand specificity of the C2 calcium-dependent lipid binding domain of cytosolic phospholipase A2, *J. Biol. Chem. 273*, 1365−1372.
21. Evans, J. H., Spencer, D. M., Zweifach, A., and Leslie, C. C. (2001) Intracellular calcium signals regulating cytosolic phospholipase A2 translocation to internal membranes, *J. Biol. Chem. 276*, 30150−30160.
22. Clark, J. D., Schievella, A. R., Nalefski, E. A., and Lin, L. L. (1995) Cytosolic phospholipase A2, *J. Lipid Mediat. Cell Signal 12*, 83−117.
23. Hegen, M., Sun, L., Uozumi, N., Kume, K., Goad, M. E., Nickerson-Nutter, C. L., Shimizu, T., and Clark, J. D. (2003) Cytosolic phospholipase A2alpha-deficient mice are resistant to collagen-induced arthritis, *J. Exp. Med. 197*, 1297−1302.
24. Perisic, O., Fong, S., Lynch, D. E., Bycroft, M., and Williams, R. L. (1998) Crystal structure of a calcium-phospholipid binding domain from cytosolic phospholipase A2, *J. Biol. Chem. 273*, 1596−1604.
25. Kunkel, T. A., Roberts, J. D., and Zakour, R. A. (1987) Rapid and efficient site-specific mutagenesis without phenotypic selection, *Methods Enzymol. 154*, 367−382.
26. Nalefski, E. A., and Falke, J. J. (1998) Location of the membrane-docking face on the Ca2+-activated C2 domain of cytosolic phospholipase A2, *Biochemistry 37*, 17642−17650.
27. Hooft, R. W., Sander, C., and Vriend, G. (1996) Positioning hydrogen atoms by optimizing hydrogen-bond networks in protein structures, *Proteins 26*, 363−376.
28. Nielsen, J. E., and Vriend, G. (2001) Optimizing the hydrogen-bond network in Poisson−Boltzmann equation-based p*K*(a) calculations, *Proteins 43*, 403−412.
29. Alexov, E. G., and Gunner, M. R. (1997) Incorporating protein conformational flexibility into the calculation of pH-dependent protein properties, *Biophys. J. 72*, 2075−2093.
30. Madura, J. D., Briggs, J. M., Wade, R. C., Davis, R. C., Luty, B. A., Ilin, A., Antosiewicz, J., Gilson, M. K., Bagheri, B., Scott, L. R., and McCammon, J. A. (1995) Electrostatics and Diffusion of Molecules in Solution: Simulations with the University of Houston Brownian Dynamics Program, *Comput. Phys. Commun. 91*, 57−95.
31. Sitkoff, D., Sharp, K., and Honig, B. H. (1994) Accurate Calculation of Hydration Free Energies Using Macroscopic Solvent Models, *J. Phys. Chem. 98*, 1978−1988.
32. Richards, F. M. (1977) Areas, volumes, packing and protein structure, *Annu. Rev. Biophys. Bioeng. 6*, 151−176.
33. Antosiewicz, J., McCammon, J. A., and Gilson, M. K. (1994) Prediction of pH-dependent properties of proteins, *J. Mol. Biol. 238*, 415−436.
34. Antosiewicz, J., McCammon, J. A., and Gilson, M. K. (1996) The determinants of pK_a's in proteins, *Biochemistry 35*, 7819−7833.
35. Varma, S., and Jakobsson, E. (2004) Ionization states of residues in OmpF and Mutants: Effects of Dielectric Constant & Interactions between Residues, *Biophys. J. 86*, 690−704.
36. Jorgensen, W. L., and Tirado-Rives, J. (1988) The OPLS potential functions for proteins: energy minimizations for crystals for cyclic peptides and crambin, *J. Am. Chem. Soc. 110*, 1657−1666.
37. Falke, J. J., Drake, S. K., Hazard, A. L., and Peersen, O. B. (1994) Molecular tuning of ion binding to calcium signaling proteins, *Q. Rev. Biophys. 27*, 219−290.
38. Dwyer, J. J., Gittis, A. G., Karp, D. A., Lattman, E. E., Spencer, D. S., Stites, W. E., and Garcia-Moreno, E. B. (2000) High apparent dielectric constants in the interior of a protein reflect water penetration, *Biophys. J. 79*, 1610−1620.
39. Sham, Y. Y., Muegge, I., and Warshel, A. (1998) The effect of protein relaxation on charge−charge interactions and dielectric constants of proteins, *Biophys. J. 74*, 1744−1753.
40. Schutz, C. N., and Warshel, A. (2001) What are the dielectric "constants" of proteins and how to validate electrostatic models? *Proteins 44*, 400−417.
41. Murray, D., and Honig, B. (2002) Electrostatic control of the membrane targeting of C2 domains, *Mol. Cell 9*, 145−154.
42. Verdaguer, N., Corbalan-Garcia, S., Ochoa, W. F., Fita, I., and Gomez-Fernandez, J. C. (1999) Ca(2+) bridges the C2 membrane-binding domain of protein kinase Calpha directly to phosphatidylserine, *Embo J. 18*, 6329−6338.
43. Conesa-Zamora, P., Lopez-Andreo, M. J., Gomez-Fernandez, J. C., and Corbalan-Garcia, S. (2001) Identification of the phosphatidylserine binding site in the C2 domain that is important for PKC alpha activation and in vivo cell localization, *Biochemistry 40*, 13898−13905.
44. Ochoa, W. F., Corbalan-Garcia, S., Eritja, R., Rodriguez-Alfaro, J. A., Gomez-Fernandez, J. C., Fita, I., and Verdaguer, N. (2002) Additional binding sites for anionic phospholipids and calcium ions in the crystal structures of complexes of the C2 domain of protein kinase calpha, *J. Mol. Biol. 320*, 277−291.
45. Bolsover, S. R., Gomez-Fernandez, J. C., and Corbalan-Garcia, S. (2003) Role of the Ca^{2+}/phosphatidylserine binding region of the C2 domain in the translocation of protein kinase Calpha to the plasma membrane, *J. Biol. Chem. 278*, 10282−10290.
46. Frazier, A. A., Wisner, M. A., Malmberg, N. J., Victor, K. G., Fanucci, G. E., Nalefski, E. A., Falke, J. J., and Cafiso, D. S. (2002) Membrane orientation and position of the C2 domain from cPLA2 by site-directed spin labeling, *Biochemistry 41*, 6282−6292.

BI0482405